The Wake of St. Vincent

RONALD B. SMITH, ARTHUR C. GLEASON, AND PAUL A. GLUHOSKY

Yale University, New Haven, Connecticut

VANDA GRUBIŠIĆ

National Center for Atmospheric Research, Boulder, Colorado

(Manuscript received 12 March 1996, in final form 29 July 1996)

ABSTRACT

The island of St. Vincent and the other Windward Islands in the southeastern Caribbean were chosen as a field site for the study of weak mountain wakes. By the authors' definition, a ''weak wake'' forms when the potential vorticity generated by a mountain is not strong enough to advect itself into eddies; rather, it is simply advected downstream by the ambient flow. *GOES-8* and Landsat sunglint images unambiguously revealed that the mountainous Windward Islands have remarkably long straight wakes. The length of St. Vincent's wake exceeds 300 km although its width is only 20 km. Near the islands, the wake structures reflect the details of the island topography. These wakes do not exhibit any obvious diurnal effect.

Boat surveys in the lee of St. Vincent confirmed the existence of features seen in the images: the sharp wake boundary, the small valley-induced jet embedded in the near wake, and the absence of any reverse flow. Aircraft surveys gave evidence of descent over the island and showed that the wake air is relatively warm and dry. The length of the wake *(L)* agrees with the formula $L = H/2C_D$ (where H is the wake depth and C_D is the surface drag coefficient), implying that the reacceleration of the wake air is caused by the ambient streamwise pressure gradient rather than by lateral entrainment of momentum or geostrophic adjustment.

Two numerical models were used to simulate St. Vincent's wake, a single-layer hydrostatic model and a 3D nonhydrostatic model. Both models indicated that air descent, acceleration, wave breaking, and weak potential vorticity generation occur over the island, causing a long straight wake.

1. Introduction

Mountain wakes are significant in dynamical meteorology because they relate to mountain drag and because wakes can influence meteorological events downstream of their generating terrain. For the present purposes, we define the mountain wake to be composed of air parcels with modified Bernoulli constant or potential vorticity (PV). This modification takes place when the air parcels are in the vicinity of a mountain, by wave breaking or other dissipative processes (Smith 1989a,b; Schar 1993). This wake definition, together with the material conservation of PV, means that the wake will behave like a streakline, that is, a locus of points in a fluid that has passed through these dissipative zones. In unsteady flow, the wake will be a complicated region but will comprise the same air parcels that would contain a dye if dye was added continuously in the dissipative wave breaking regions.

Mountain wakes should not be confused with lee waves. Because of their propagation properties, mountain-induced internal gravity waves may also be found in the lee of an obstacle. In general, however, the region containing propagating lee waves is far more widespread than the wake, both laterally and vertically. Mountain lee waves may also be carrying off momentum associated with mountain drag, but unlike the wake, the lee waves are not fundamentally related to a dissipative process and they do not contain a modified Bernoulli constant or PV.

The theory of mountain wakes has recently been developed within the context of a shallow-layer stratified fluid model (Schär and Smith 1993a,b; Smith and Smith 1995; Grubišić et al. 1995). According to this model, when a mountain ridge of sufficient height has a cross-flow orientation, the flow will accelerate over the ridge crest to a supercritical speed followed by a hydraulic jump. The dissipation in this jump will decrease the Bernoulli constant of the fluid passing through it and will generate banners of positive and negative potential vorticity at the ends of the jump. If the vorticity generation is weak, it will be carried directly downstream by the ambient flow. If the vorticity generation is strong, it may advect itself into eddies. According to Grubišić

Corresponding author address: Prof. Ronald B. Smith, Department of Geology and Geophysics, Kline Geology Laboratory, Yale University, P.O. Box 208109, New Haven, CT 06520-8109.
E-mail: ronald.smith@yale.edu

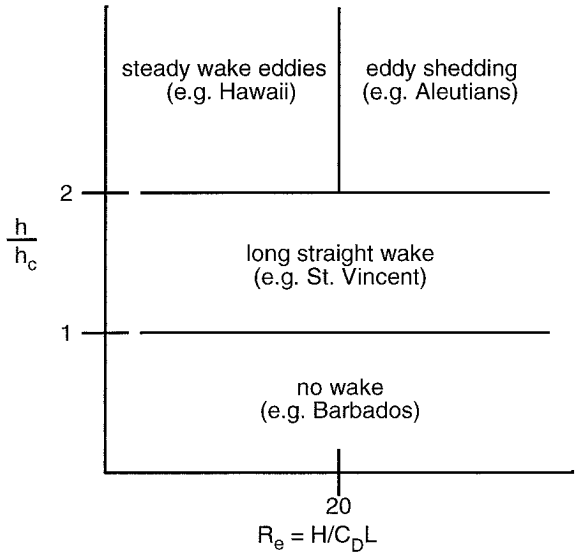

FIG. 1. A wake regime diagram with coordinates related to the mountain height and a bottom friction parameter. Four wake regimes are indicated. The structure of this diagram was suggested by the work of Schär and Smith (1993) and Grubišić et al. (1995). The exact locations of the regime boundaries are unknown.

et al. (1995), the self-advection may operate in two ways. With little bottom friction, the wake will become unstable and periodic eddy shedding will occur. With more bottom friction, a pair of steady counterrotating eddies will form in the lee. Bottom friction can also be a source of PV, but in the parameter space examined by Grubišić et al. (1995) this was a minor effect. Its primary role was to control the stability of the wake.

Four possible mountain flows are summarized in the schematic regime diagram (Fig. 1), whose general form is suggested by the work of Schär and Smith (1993a) and Grubišić et al. (1995). This diagram includes two independent control parameters: the ratio of mountain height h to the critical height for wave breaking h_c and a special Reynolds number derived for shallow flow with bottom friction (Re $= H/(C_DL)$. In this expression, H is the layer depth, C_D is the friction coefficient at the lower boundary, and L is a characteristic horizontal scale. If the mountain height is less than the critical height for wave breaking, no PV will be created and no wake will exist. For h slightly greater than h_c, a small amount of PV will be generated and will be carried downstream. We refer to this pattern as a ''weak wake,'' as the PV is too weak to advect itself into closed eddies. For h considerably greater than h_c, strong PV generation and self-advection of vorticity into eddies will occur. Depending on the shallow-water Reynolds number, these eddies will either form stationary lee eddies or shed periodically and drift downstream.

Observations of mountain wakes have thus far been done most effectively near mountainous islands. The isolated geometry, among other reasons, simplifies the observing problem for islands. Numerous examples of ''strong wake'' eddy shedding have been seen in cloud patterns from satellite (Hubert and Krueger 1962; Chopra 1973; Etling 1989; etc.), although no in situ measurements have been reported. One well-known example of shedding eddies is the wakes of the Aleutian Islands during steady northerly flow. The wake of Hawaii was surveyed with a research aircraft in 1990, revealing a pair of large quasi-stationary eddies in the lee (Smith and Grubišić 1993).

The objective of this study is to verify the existence of weak mountain wakes in the earth's atmosphere and to learn something about their dynamics.

2. The island of St. Vincent

After a broad search, the Caribbean Windward Islands, including the island of St. Vincent, were selected as a test site for these investigations. These islands have several advantages for wake studies, as discussed below.

The Windward Islands in the Lesser Antilles form a north–south oriented chain of volcanic islands from 12° to 16°N along the 61°W meridian. This chain includes Dominica, Martinique, St. Lucia, St. Vincent, and Grenada. The mountainous terrain of these islands is shown in the view-from-the-east profile given in Fig. 2. As their name implies, the Windward Islands lie in a belt of steady easterly trade winds. Except for the island of Barbados, there are no obstacles upstream of the Windwards for 4000 km. The peaks of the islands reach about halfway to the altitude of the trade wind inversion.

The island of St. Vincent has the simplest topography of the Windward Islands. The cone of Soufriere at the north end of the island reaches to about 1100 m, while the irregular ridge in the middle and southern part of the island approaches 1000 m. A gap, just to the south of Soufriere, is evident in Figs. 2 and 3. Mount Soufriere is known to have erupted twice in recent times. In both instances, observers used the shape of the spreading ash clouds to interpret the local airflow patterns. Flammarion (1874) noted that the ash falls on Barbados following the 30 April 1812 Soufriere eruption gave evidence of the countertrades (i.e., westerlies) aloft. The eruption on 17 April 1979 was examined with lidar (Fuller et al. 1982) and with photography (Barr 1982) for evidence of nonuniform stratification in the local atmosphere. Neither the 1812 nor the 1979 observations gave evidence of St. Vincent's wake.

St. Vincent and the other Windward Islands have a number of advantages for wake studies. As with any island, the surrounding ocean surface simplifies the airflow geometry and allows boat and low-level aircraft surveys. The ocean surface also acts as a flow visualization medium, as the reflection of electromagnetic radiation from the sea surface is affected by short-wavelength wind-induced ocean waves. During Northern Hemisphere winter, the Windward Island region is generally free of midlevel and cirrus clouds that could obscure satellite images. The low latitude of these islands

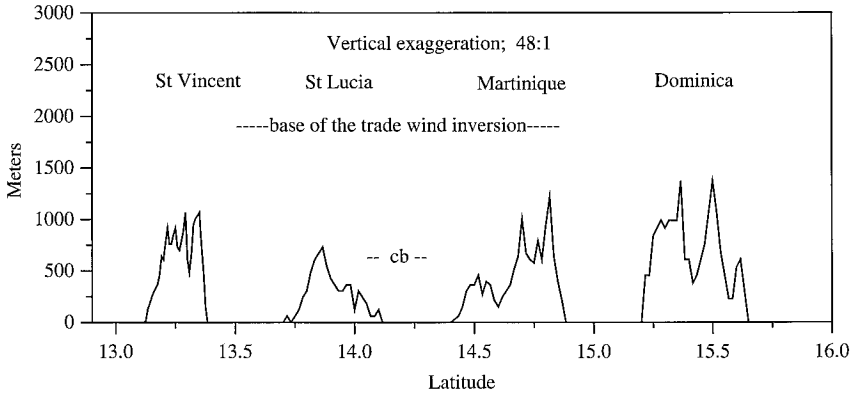

FIG. 2. Terrain profile of the four Windward Islands from 13° to 16°N latitude. The vertical scale is exaggerated. The altitudes of cloud base (cb) and the trade wind inversion are indicated.

also makes it possible to obtain reflected light "sunglint" images from equatorially orbiting geostationary satellites. The low-lying island of Barbados, about 180 km upstream of St. Vincent, provides a convenient site for balloon soundings. An additional advantage of the Windward Island region is that the properties of the local trade wind convective boundary layer have been extensively studied in the BOMEX Project (see Siebesma and Cuijpers 1995 and references therein).

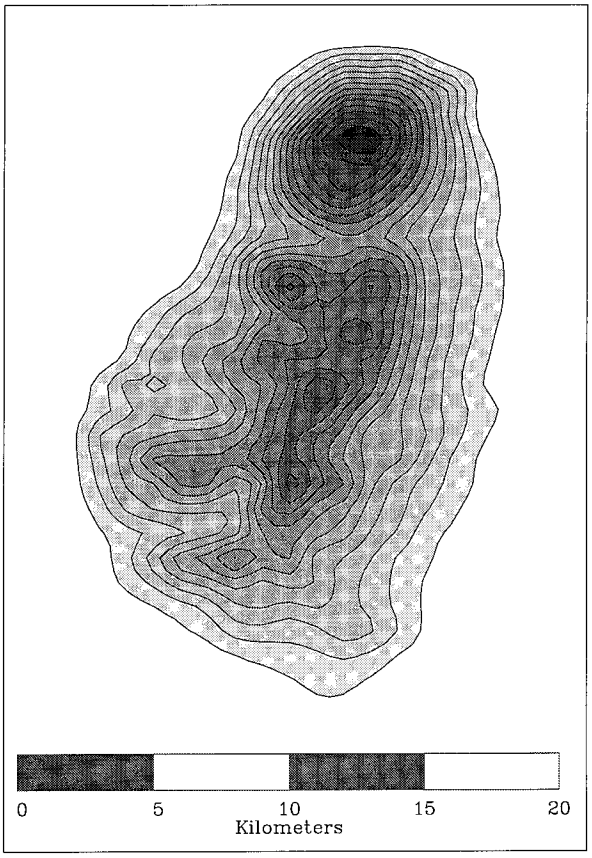

FIG. 3. The smoothed topography of St. Vincent. The contour interval is 70 m. The actual maximum height of Soufriere on the north end of the island is 1178 m.

There have been four previous studies of wakes in the Lesser Antilles. Strong et al. (1974) discussed sunglint from these wakes as they appeared in images from the Very High Resolution Radiometer instrument on *NOAA-2*. Cram and Hanson (1974) used *ERTS-1* images to argue that the wakes are caused by the mountains on the islands. Needham (1976) compared Landsat sunglint images of St. Vincent with images of Pulu Bawean in the Java Sea. Fett and Bohan (1981) discussed a Defense Meteorological Satellite Program and a Landsat image of St. Vincent. The recent improvement in satellite sensors and image analysis software, together with in situ measurements and numerical models will enable us to extend these earlier studies and learn more about island wakes.

3. Sunglint patterns

a. GOES imagery

Under favorable conditions, satellite images of sunglint provide a useful tool for observing wind patterns over the sea (Cox and Munk 1954a,b; Fett and Burk 1981; Fett and Isaacs 1979; Fett and Rabe 1976; Khattak et al. 1991; Johnson et al. 1994; Maul and Gordon 1975; McClain and Strong 1969; Strong and Ruff 1970). As shown by Cox and Munk (1954a), the probability distribution function for ocean wave slopes is nearly Gaussian with a variance (σ^2) that is proportional to the wind speed. For example, a wind speed of 10 m s^{-1} will give rise to a wave slope variance of $\sigma^2 = 0.04$, while a 5 m s^{-1} wind will give half that variance. The slope variance controls how the sun's direct beam is reflected from the sea surface. In an island wake, with slow winds, the relatively smooth sea surface will give increased specular reflection and decreased diffuse reflection. The opposite is true for the rougher sea surface regions outside the wake, which experience a higher windspeed. The primary disadvantage of the sunglint method is that

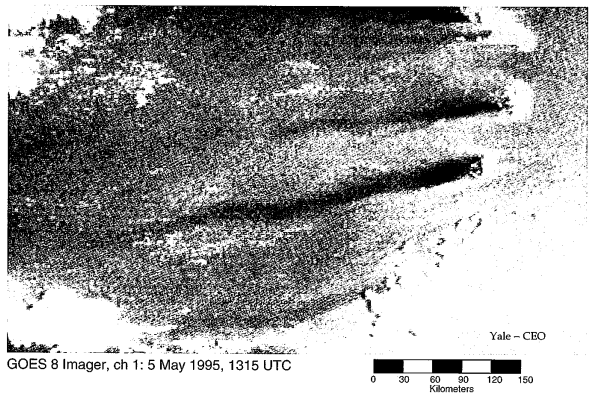

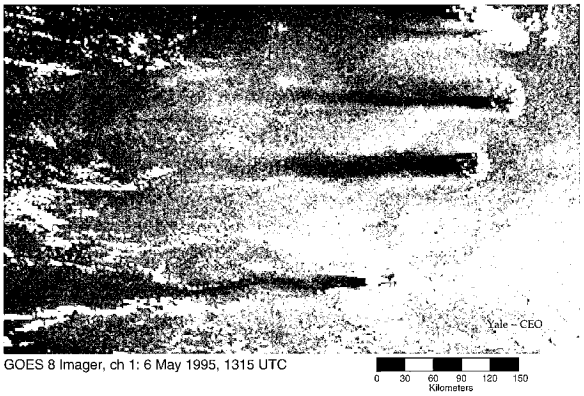

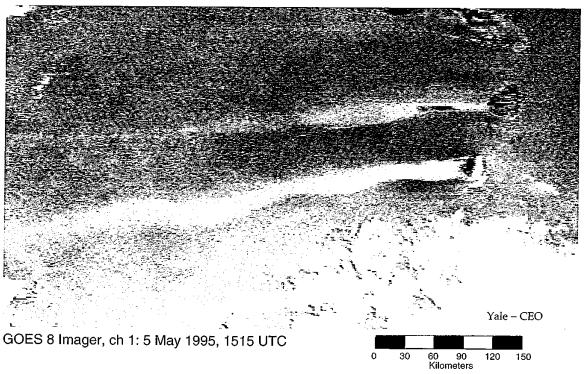

FIG. 4. *GOES-8* channel-1 (visible) images of the Windward Islands showing patterns of sea surface sunglint at two different illumination angles on 5 May 1995: (a) 1315 UTC and (b) 1515 UTC. Martinique is at the northern edge of the frame. Grenada is totally obscured by clouds in the southern part of the frame.

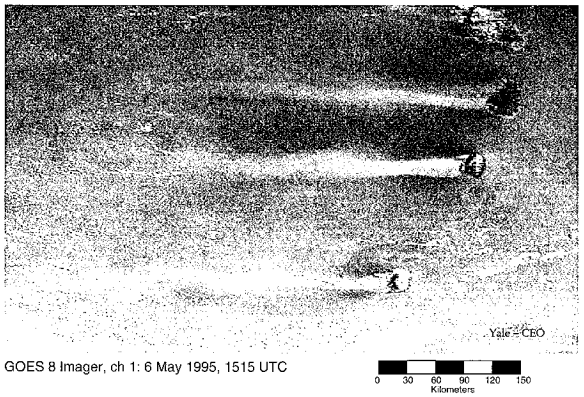

FIG. 5. Similar to Fig. 4 but on 6 May 1995: (a) 1315 UTC and (b) 1515 UTC. Martinique is partly visible at the northern edge of the scene. The Peninsula of Paria near Trinidad is located near the sourthern edge of the scene.

the appearance of an island wake is sensitive to the sun–satellite geometry, and thus it will change rapidly with time of day and with location within a particular scene. When an island is near to the specular point, its wake will appear bright while the surrounding ocean surface will be relatively darker. When the island is farther away from the specular point, the wake will be darker than the surrounding rougher sea surface. There is one useful aspect of this angle sensitivity. A dramatic change in wake appearance over a 2-h interval provides unambiguous evidence that ocean wave slopes are being observed—as opposed to whitecaps, suspended particles or plankton, atmospheric haze, or clouds—all of which give primarily diffuse reflection, that is, reflection that is relatively insensitive to sun angle.

Figures 4–6 show pairs of *GOES-8* sunglint images of the Windward Islands recorded during May 1995. One striking aspect of these images is the shift from a dark to a bright wake over a 2-h interval. This shift provides evidence that we are seeing the wake expressed by specular sunglint. In all three cases, the wake length exceeds 300 km. The wake edges remain quite sharp, even at a distance of 200 km downstream from the islands. The island of Barbados, which lies just off the images to the right, generates no wake. We will verify this result in section 3b. The lack of a wake from Barbados is presumably due to its lack of substantial mountains.

The wakes in Figs. 4–6 are remarkably free of clouds, even when the wake passes through dense clusters of tradewind cumuli. On the other hand, there is a tendency for a thin row of cumulus clouds to occur just along the wake boundaries, as has been noted by previous authors.

The pair of GOES images in Fig. 4 shows that the sinusoidal waviness in the far wake has moved noticeably westward over a 2-h interval. This pattern shift corresponds to a speed of 6–8 m s^{-1}. Such a drift speed agrees with the range of speeds measured at the 850-mb level by the Barbados balloon soundings, suggesting that the motion of this feature could be caused by atmospheric advection. In any case, the rapid movement of the waviness confirms that the sunglint wake of St. Vincent is an atmospheric feature, not an oceanic feature such as a surface oil slick. A surface slick could move little faster than the ocean currents (e.g., a few centimeters per second).

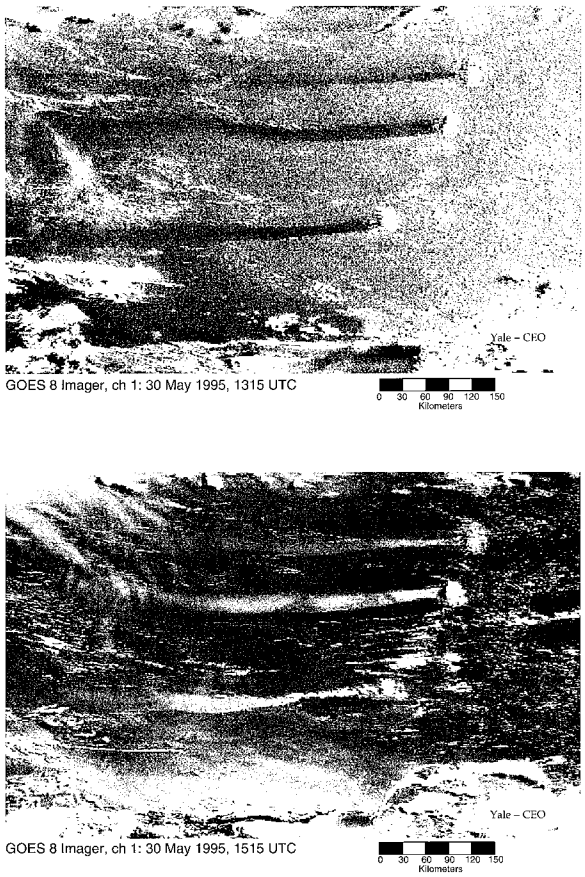

FIG. 6. Similar to Fig. 4 but on 30 May 1995. (a) 1315 UTC and (b) 1515 UTC.

b. Landsat imagery

Figure 7 shows a composite strip of four Landsat multispectral scanner (MSS) scenes from 24 March 1986. At 1000 LST (1400 UTC), when the image was acquired, the sun and satellite were in positions leading to a dark wake in sunglint. While the image does not extend as far downstream as Figs. 4–6 do, the smaller pixel size of 80 m allows many details to be seen. These details can be made clearer by zooming on each island as is done in Figs. 8 and 9.

It is interesting to compare the near-field sunglint-derived wake structure with the island profiles in Fig. 2. The island of Dominica (Fig. 9a) generates a broad wake. Within the wake, two small bright regions pointing westward from the coast are evident. We interpret these regions as wind jets downstream of the two passes in the Dominican ridgeline shown in Fig. 2. Also evident are bright patches north and south of the island. These patches arise from the airflow acceleration around the northern and southern tips of the island. The island of Martinique (Fig. 9b) generates a wake from the large mountains in the north and a weak wake from the southern hills. In the middle of the northern wake is a wind jet corresponding to the pass (latitude 14.7°N) shown in Fig. 2. St. Lucia (Fig. 9c) generates a wake from the higher mountains on the southern part of the island. The wake, and the ridgeline altitude, diminish toward the north.

The wake of St. Vincent is shown in Fig. 9d. The north–south dimension of the wake corresponds approximately to the entire length of the island as, according to Fig. 2, the mountain ridge itself extends from nearly tip to tip. The wake is very well defined, with sharp edges, over the entire 140-km portion of the wake shown in this figure. The wake is free of clouds, even where it penetrates through a field of cumulus clouds in the western part of the image. A region of decelerated winds is seen upstream of the island, probably caused by orographic blocking. Regions of accelerated winds are seen just outboard and downstream of the north and south tips of the island. Such a feature could be called a ''corner wind.''

Figure 8 shows a more detailed Landsat zoom of St. Vincent. For even greater spatial resolution, we have used a Landsat thematic mapper (TM) image taken at the same time as the MSS images in Figs. 7 and 9a–d. The TM image has a pixel size of 30 m. The wake boundaries and the brighter acceleration zones north and south of the island are clearly seen. A wind jet is present, emanating from the pass just south of Soufriere. The volcano itself is evident in the image, as is a small river indicating the position of the pass.

One interesting detail in this high-resolution image is the periodic wavelike brightness pattern along the northern shear line, just west of the island. A very similar feature occurred in the Landsat image of St. Vincent from 1973, discussed by Fett and Bohan (1981). This feature is probably a modification of ocean surface wave amplitudes by ocean internal waves. The wavelength of these waves is about 1.5 km.

Two other Landsat MSS images of St. Vincent have been analyzed: 3 January 1986 and 5 October 1987 (not shown). Both of these images show well-defined sunglint wakes, but in neither case are the wakes as long and clear as in the 24 March 1986 case shown in Figs. 8 and 9d. The 3 January case requires careful image enhancement to make the wake evident. This difference is due to a less favorable sun angle for sunglint. In October, and especially in January, the sun is in the Southern Hemisphere. From the location of the satellite over the island of St. Vincent at 14°N, the point of specular reflection is well south of the island.

For comparison with the mountainous islands discussed above, we show a Landsat MSS image of flat-lying Barbados in Fig. 9e. Although the sun–satellite geometry is appropriate for sunglint at the time of the image, no sunglint wake is seen. This is not a surprise as the highest point on Barbados, Mt. Hillaby, is only 336 m high, about one-third the height of the volcanic islands in the main Windward Island chain (Fig. 2). It

is well known that Barbados generates a long trail of cumulus clouds extending westward in the afternoon, but this feature is not a wind wake as we have defined it. It also has a ''thermal'' wake as discussed in section 6b. Apparently, neither the roughness nor the warmth of the Barbados surface produces a significant wind wake.

In summary, the temporal comparison of GOES images in Figs. 4–6 and the island-by-island comparison of Landsat images in Figs. 7–9 indicate that the Windward Islands have long mountain-generated atmospheric wakes made evident by a smoother sea surface. Near to the islands, the detailed structures of the wakes reflect the mountain and pass geometry of the island terrain.

4. Field observations

In order to verify the interpretation of sunglint patterns and to determine some physical characteristics of the wake, a short field program was carried out near St. Vincent from 22 January to 15 February 1995. Due to limited funds, the goal of the field program was restricted to the identification of the gross properties of the near-island airflow using simple portable instruments. Two types of observations were carried out: small boat surveys of wind in the near wake and aircraft measurements of temperature and humidity over the island and in the near wake. In addition, qualitative observations of cloud drift, wind strength, and ocean wave patterns were made from coastal vantage points.

In order to map out the pattern of surface wind in the wake over the sea, a 20-ft skiff was outfitted with a wind vane and a cup anemometer, a laptop computer, and a global positioning system (GPS) unit. During the survey, the boat maintained a speed of about 8 knots (5m s^{-1}). The boat-relative wind was measured by the anemometer every 2 s while the GPS system gave the boat speed and direction over the earth. With the assumption that boat heading was equal to the direction of the boat movement vector, the absolute wind could be easily determined. One survey was accomplished across the southern shear line, and four across the northern shear line. The detailed structure and position of the shear lines varied from day to day due to changes in the trade wind flow direction. The clearest steadiest example of northern shearline structure was found on 6 February 1995 (Fig. 10). At the beginning point of the survey (latitude 13.28°N), the measured winds were light and variable. A short distance to the north (13.29°N), a sharp-edged jet of wind was encountered that continued to be felt until reaching a latitude of 13.35°N. Weak winds then prevailed until the accelerated trade winds were encountered at 13.38°N. Based on the appearance of the sea surface between the boat and the coast, we could identify the jet between 13.29° and 13.35°N as a gap-induced feature. The calm region from 13.35° to 13.38°N could be clearly identified as the wake behind Soufriere.

In addition to the boat surveys, three aircraft surveys were carried out. These missions used a Cessna 402 twin-engine propeller aircraft equipped with redundant thermocouples for measuring temperature, a Vaisala Humitter for humidity, redundant bellows pressure sensors, and a GPS unit. A laptop computer was used as a datalogging system. Each mission lasted about 1 h and was composed of three parts: an upstream thermodynamic sounding, a level leg downwind across the island, and a low-level north–south leg across the wake. Data from the flight on 10 February 1995 are shown in Fig. 11.

The upstream sounding (Fig. 11a) gives temperature and humidity as a function of pressure altitude from 600 to 3000 m. The base of the sounding at $z = 600$ m is near to the cumulus cloud base, and we can assume that the lapse rate is adiabatic below this level. This assumption would give a surface temperature of 26°C, a reasonable value for February in this tropical region. Above 600 m, the temperature decreases with a lapse rate of $dT/dz = -6.1$°C km^{-1} until the inversion is reached at 2400 m. Above the inversion lies an isothermal layer. Observed cumulus clouds had tops from 1600 to 2400 m altitude.

The relative humidity in the cumulus layer decreased from 60% at 600 m to 25% at 2400 m. Above the inversion, the humidity is less than 10%, the lower limit of accuracy for our sensor. These thermodynamic profiles agree qualitatively with the Barbados sounding on the same day and with soundings by previous investigations in this region (e.g., Siebesma and Cuijpers 1995). These profiles will be used in section 6 to estimate the role of stratification in wake formation and in section 7 to set the upstream conditions for two numerical models.

The cross-island leg is shown in Fig. 11b. The bottom panel shows that the aircraft maintained a constant altitude of 1700 m, slightly less than twice the mountain height. Due to clouds over the upwind side of the island, the cross-island leg could not be done safely at a lower altitude. Both the temperature and relative humidity show evidence of descending air beginning upstream of the ridge crest. The temperature climbed by about 3°C in the wake, and the relative humidity fell from 58% to 30%. Using the upstream profiles of temperature and mixing ratio in Fig. 11a, these thermodynamic changes would be consistent with an air parcel descent of at least 500 m. The level of turbulence on the cross-inland leg was light to moderate. If there is strong turbulence present over the lee slopes of St. Vincent, it is probably located at an altitude below the aircraft traverse at 1700 m.

The cross-wake leg (Fig. 11c) was done at an altitude of about 470 m, slightly below cumulus cloud base and about half the mountain height (see the lowest panel in Fig. 11c). The air in the wake at this level was about 1.5°C warmer (22.0°C instead of 20.5°C) than the air to the north and south of the wake. The mixing ratio

FIG. 7. A Landsat MSS five-scene composite showing sunglint patterns near the Windward Islands, from Guadeloupe to Grenada, on 24 March 1986. The color representation is 421-RGB.

FIG. 8. A Landsat TM scene zoom showing sunglint patterns near St. Vincent on 24 March 1986. The pixel size is approximately 30 m. The color representation is ''true-color'' 321-RGB.

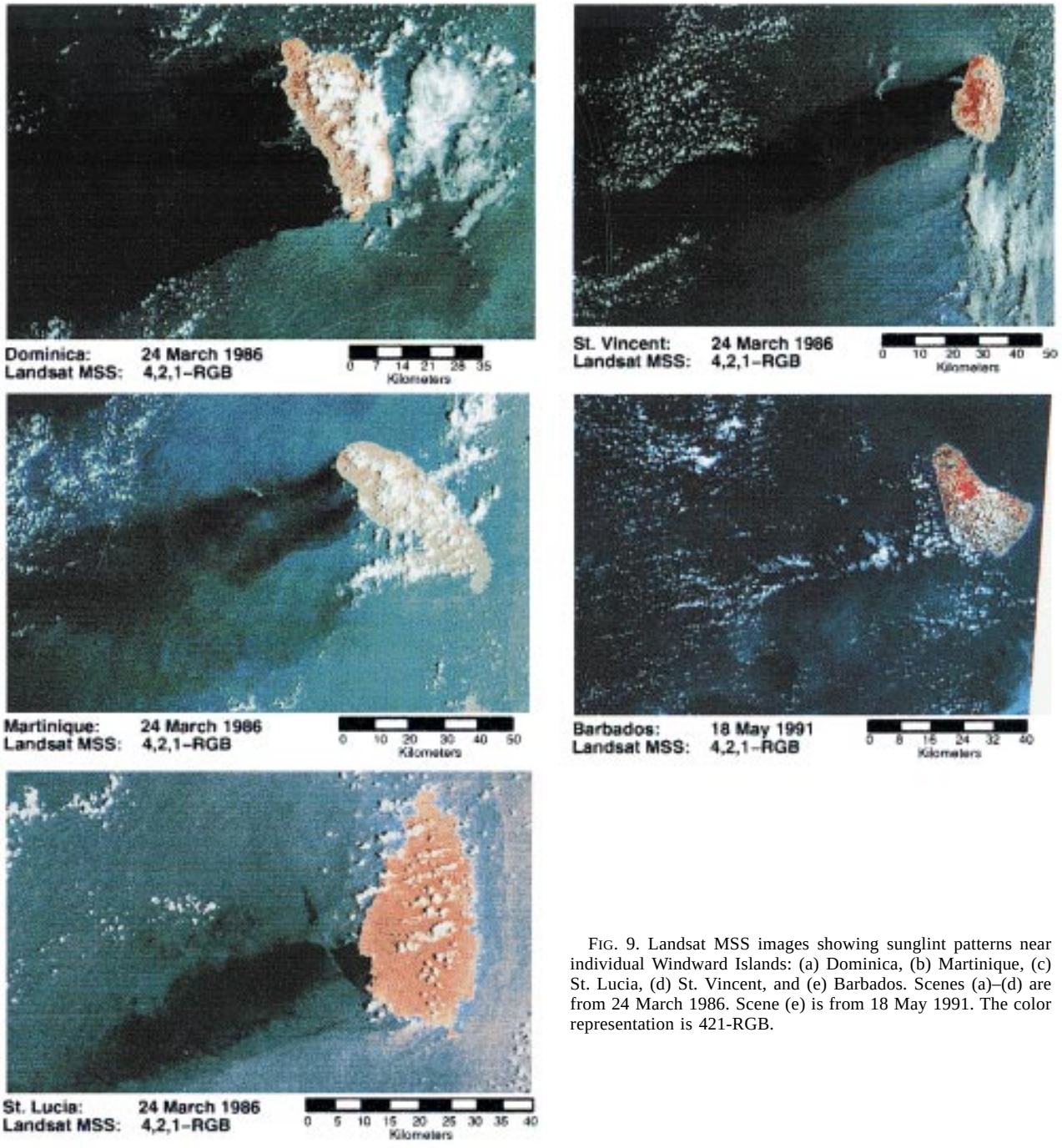

FIG. 9. Landsat MSS images showing sunglint patterns near individual Windward Islands: (a) Dominica, (b) Martinique, (c) St. Lucia, (d) St. Vincent, and (e) Barbados. Scenes (a)–(d) are from 24 March 1986. Scene (e) is from 18 May 1991. The color representation is 421-RGB.

was reduced from 11.5 to 10 g kg^{-1}. This higher temperature and lower mixing ratio would be consistent with the downward mixing of drier, potentially warmer air from aloft. The difference in virtual temperature between the wake and its environment was also about 1.5°C, indicating that the wake air was less dense than its surroundings.

The in situ observations of St. Vincent's wake could be summarized as follows. From the boat surveys, the interpretation of satellite sunglint patterns as surface wind variations was confirmed, including the lack of reverse flow and the existence of the near-wake jet, south of Soufriere. The sharpness of the sunglint wake boundary was also verified. The cross-wake aircraft surveys indicated that the wake air was warmer and drier than the air outside the wake. The cross-island aircraft survey showed descent over the mountain top and that the wake was warmer and drier than the air upstream.

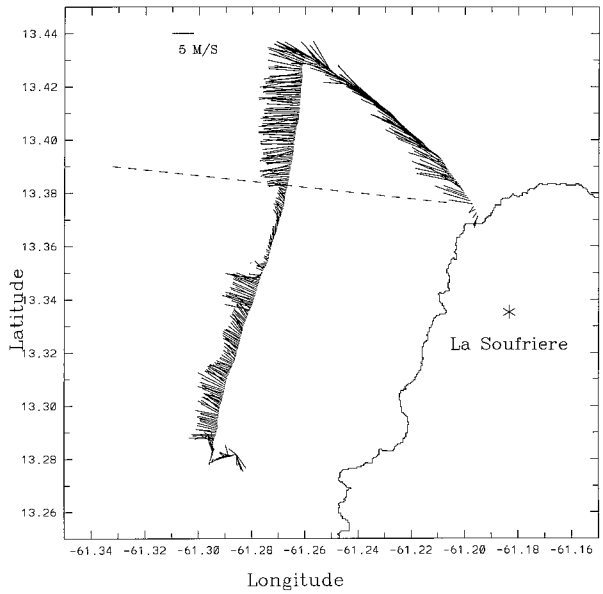

FIG. 10. Surface wind vectors near the northern edge of St. Vincent's wake as determined from a small boat survey on 6 February 1995. The northern shearline is marked with a dashed line.

5. Wave breaking and wake generation

The existence of St. Vincent's wake implies both that potential vorticity is produced and that the Bernoulli constant is decreased by dissipative processes over the island. The equivalence of these two statements is discussed by Schär and Smith (1993a, hereafter SS93a) and Schär (1993). The dissipation over the island is probably caused by one of two processes: wave breaking or boundary layer turbulence. The control of the wake by terrain height suggests, but does not prove, that gravity wave breaking is the dominant mechanism. Wave breaking is known to have a ''threshold'' behavior, where small differences in mountain height (h), wind speed (U), and stability (N) can make the difference between flows with and without breaking. This hypothesis can be checked against existing criteria for the onset and persistence of wave breaking. Because the east–west half-width of the St. Vincent terrain ($a_x \approx 4$ km) exceeds the characteristic gravity wave horizontal scale ($U/N \approx 1$ km), we apply hydrostatic theories in trying to judge the likelihood of wave breaking. Furthermore, because the horizontal aspect ratio of St. Vincent (a_y/a_x) is greater than 2, the simpler two-dimensional theory can give a useful estimate of the critical condition for the onset of wave breaking (Smith 1989c; Stein 1992; Smith and Grønås 1993). One must be careful not to apply other aspects of 2D theory to the St. Vincent problem, however. The generation of PV, upstream blocking, the downwind extent of supercritical wind flow, and wake instability are all inherently three-dimensional issues.

For environments with uniform stratification and ambient wind, wave breaking will occur for a nondimensional ridge height greater than $\hat{h} = hN/U = 0.85$ for a Witch-of-Agnesi shape (Huppert and Miles 1969). In the present case, if we choose an average lapse rate of -5.5°C km^{-1}, $U = 9$ m s^{-1}, $h = 1000$ m, we obtain the value of $\hat{h} = 1.3$, clearly suggesting wave breaking. With this lapse rate, only a wind speed in excess of 14 m s^{-1} would avoid wave breaking.

We can proceed further on the question of wave breaking by using a 2D numerical model (see section 7b) to take into account the actual upstream temperature structure. This structure is estimated from the Barbados sounding and the aircraft sounding. A calculation using the observed upstream temperature structure, a uniform wind of $U = 6.5$ m s^{-1}, and a 1-km high Witch-of-Agnesi ridge with $a_x = 4.0$ km is shown in Fig. 12. The pattern of isentropes in Fig. 12 reveals descent and rapid acceleration of a type first simulated by Clark and Peltier (1977) and derived theoretically by Smith (1985). The descent primarily involves the isentropes in the trade wind cumulus layer, not in the sharp trade wind inversion itself. This calculation indicates that the concentrated stratification in the trade wind inversion is at too high an altitude to be significantly disturbed by a 1-km high ridge for typical trade wind speeds of 5–8 m s^{-1}. Thus, the descent over the Windward Islands, leading to wave breaking and wake formation, is dependent on the buoyancy stratification in the trade wind cumulus layer beneath the inversion.

A shallow-water formulation can also be used to examine the question of wave breaking. For this purpose, we define a potential temperature thermal interface of strength $\Delta\theta$ at a height H to represent the stable stratification in the trade wind cumulus layer, the layer between 600 and 2400 m. From this layer, we estimate $\Delta\theta = 8$°C and $H = 1500$ m. These choices give a height ratio $M = h/H = 0.67$ and and a Froude number $\mathrm{Fr} = U/\sqrt{g'H} = 0.4$. These values for the nondimensional control parameters M and Fr suggest that supercritical acceleration and a hydraulic jump will occur (SS93a). Alternatively, one might choose parameters to represent the trade wind inversion itself. A layer depth of $H = 2500$ m would give a lesser $M = 0.4$ and a similar Froude number (in spite of the increased stability), rendering it less likely that supercritical flow could occur. In section 7a, the parameter sensitivity of the shallow-water model will be considered again as we use it to calculate the three-dimensional structure of the wake behind St. Vincent.

In spite of the evidence given above, that density stratification effects can cause a wake, an alternative mechanism should be considered. It is well known from the fluid dynamics literature that even in a homogeneous fluid, boundary layer separation can cause drag and generate a wake. In the case of St. Vincent, the eroding volcanic terrain is very rugged and some boundary layer separation, at least on scales of a few hundred meters, is likely. In a comparison of these two theories, the strong control of the wake by terrain height, the lack of a wake from Barbados, and the observed leeside descent

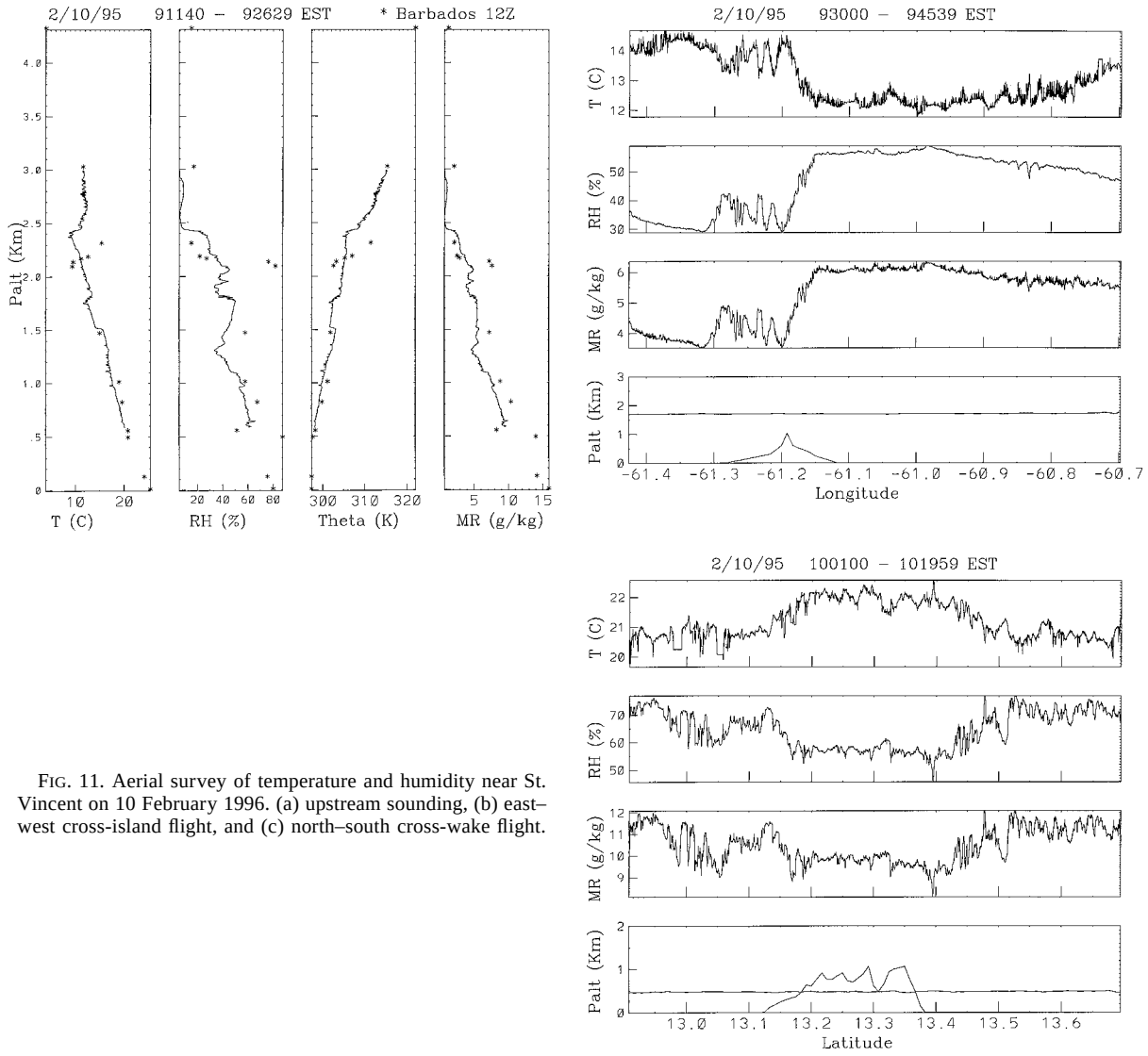

FIG. 11. Aerial survey of temperature and humidity near St. Vincent on 10 February 1996. (a) upstream sounding, (b) east–west cross-island flight, and (c) north–south cross-wake flight.

over St. Vincent would seem to favor the deep ''stratification'' mechanism over the ''boundary layer'' mechanism. Also, the lack of a diurnal effect on the wake would probably favor the deep mechanism as the diurnal variation of boundary layer structure would alter the way that separation occurs.

6. The length of the wake

a. Acceleration mechanisms

There are three mechanisms that could accelerate the wake air and restore its original momentum: classic geostrophic adjustment, acceleration by the streamwise pressure gradient, and entrainment of faster-moving air from the sides or the top of the wake. The great length of St. Vincent's wake implies that none of these mechanisms are very effective.

According to the concept of geostrophic adjustment (Blumen 1972), a subgeostrophic strip of fluid will adjust by moving laterally, that is, to the left in the Northern Hemisphere. During the lateral movement, two things happen. The original cross-stream pressure gradient accelerates the flow, and the changes in the stratification aloft weaken the cross-stream pressure gradient. Either the former or the latter mechanism will dominate the adjustment process, depending on whether the ratio $R = D/L_R$ is greater or less than unity; here D is the strip width and L_R is the Rossby radius of deformation. For our problem, D is the width of the wake; $D \approx 20$ km. The Rossby radius can be estimated from $L_R = \sqrt{g'H}\,/\,f$ where g' and H are the effective gravity and altitude of the trade wind stratification and f is the Coriolis parameter. Choosing $g' = 0.1$ m s^{-2}, $H = 1500$ m, and $f = 2\Omega \sin\phi = 0.35 \times 10^{-4}$ s^{-1} gives $L_R = 350$

km and $R = 0.06$. From this small value of R, we conclude that geostrophic adjustment of St. Vincent's wake would occur by a slight adjustment of the inversion height, with no significant acceleration of the wake air (see section 7a.2).

We now consider the acceleration of wake air by the streamwise pressure gradient. The undisturbed trade wind air beneath the inversion moves westward under a streamwise force balance between friction at the lower boundary and the streamwise pressure gradient. The slower wake air will feel the same streamwise pressure gradient, but with reduced friction. The steady acceleration process for a layer of depth H will obey

$$\rho U U_x H = -Hp_x - \rho C_D U^2, \tag{1}$$

where "x" is the streamwise coordinate, U is the flow speed, and C_D is the surface drag coefficient. The downstream pressure gradient force Hp_x can be related to the undisturbed flow speed U_∞ according to $p_x = -\rho C_D U_\infty^2$. Equation (1) has an exact solution, but it is simpler to use the linearized version. For a small perturbation $u' = U - U_\infty$, (1) becomes

$$u'_x = -L^{-1}u', \tag{2a}$$

where

$$L \equiv H/(2C_D) \tag{2b}$$

is a characteristic wake decay scale. Equation (2) admits a solution

$$u'(x) = u'(0)e^{-x/L}. \tag{3}$$

For the present estimates, we use drag coefficients based on the wind speed at an altitude of 100 m. For three surfaces, sea, flat land, and forest, accepted values of the drag coefficient are $C_{D_{100}} = .0012$, .0015, and .0057, respectively. Choosing $H = 1500$ m, the three values for drag coefficient give three corresponding values for L: 624, 500, and 132 km. The predicted value of L for the sea (624 km) is somewhat greater than the satellite observations discussed in section 3. A choice of $H = 1000$ m would give $L = 416$ km, in better agreement (see also section 7a.3).

It is more difficult to estimate the magnitude of lateral and top entrainment of momentum into the wake. The entrainment of momentum from aloft due to cumulus clouds is probably negligible as, according to Figs. 4–6, there are no cumulus clouds in the wake. The shear-induced mixing between the slow wake air and the ambient air above may be significant, however. The interface zone between these two streams would have to thicken to approximately 400 m before the average Richardson number would exceed unity and the shear-induced mixing could cease (Turner 1973). Lateral mixing may be negligible as the wake edges appear to remain sharp in the sunglint images (Figs. 4–6).

The striking aspect of the sunglint imagery is that the wake of St. Vincent is quite long in comparison with the lateral dimension of the island, a ratio of $L/a_y = 15$ or greater. The essential point is that because lateral mixing of momentum plays little role, the wake length is not controlled by the lateral mountain width. To illustrate this point, imagine two hypothetical situations under the assumption that Eqs. (2) and (3) govern the wake decay. Consider first a short mountainous island like St. Vincent and second, a longer mountain ridge, located on a forested continent. In the former case, let $a_y = 20$ km, $C_D = .001$, and $H = 1$ km, so that $L = 500$ km and $L/a_y = 25$. In the latter case, let $a_y = 100$ km, $C_D = .005$, and $H = 1$ km, so $L = 100$ km and $L/a_y = 1$. This wide variation in the ratio L/a_y contrasts with the wakes in classic 2D cylinder flow where the ratio varies only between 2 and 5, because of the controlling influence of lateral viscosity.

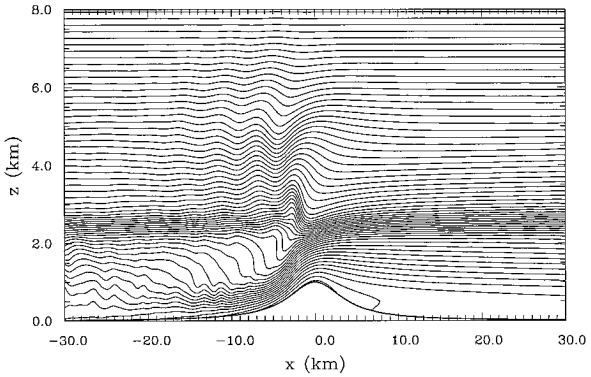

FIG. 12. A numerical two-dimensional steady-state solution to stratified airflow across an ideal 1-km Witch-of-Agnesi ridge with an upstream temperature profile, typical of the trade winds in the St. Vincent region. Potential temperature is contoured with an interval of 0.5 K. The lowest isentrope is 297 K. The upstream velocity is 6.5 m s^{-1}. Only the inner 60 km of the full 120-km domain is shown.

If the above argument is correct, the large length to width ratio of St. Vincent's wake is only possible because of the low latitude and small cross-flow dimension of the island and the smoothness of the surrounding ocean surface.

b. An alternative interpretation

The extraordinary length of the wake described in section 3 is subject to an alternative explanation. According to Deardorff (1976) and Fett and Burk (1981), boundary layer air that has been warmed as it passes over a hot island surface can stabilize the lower tens of meters of the atmosphere when it passes back over the cool ocean surface in the lee. This stabilization could reduce the wind stress and the generation of short gravity waves on the ocean surface. For sunglint patterns, this stabilization process would be indistinguishable from our conception of a deeper wake with a significant momentum deficit. The plume of heated boundary layer air would be carried downstream just like our proposed weak PV banners.

A good example of heat island effect is DeSouza's

aircraft study of Barbados (1972; see also Garstang et al. 1975). At midday, he observed a leeside plume of warm air at an altitude of 400 m, with a temperature excess of about 1°C. The plume is entirely absent from dusk until dawn. Our midday St. Vincent cross-wake leg (Fig. 11c) found a somewhat larger temperature excess at a similar altitude.

Unfortunately, the thermal hypothesis for generation of a smooth sea surface wake contradicts the satellite evidence, particularly 1) the lack of diurnal effect on the wake, and 2) the lack of a wake behind Barbados. The lack of diurnal effect is especially telling. Our wake images (Figs. 4–9) were taken only about 3–4 h after sunrise. If no wake was formed at night, the observed wake in the late morning could not be longer than 100 km. In fact, the wake length exceeds 300 km. Concerning Barbados, we know it has a thermal plume and yet we cannot detect a sunglint wake. Thus Barbados provides a counterexample to the thermal wake hypothesis.

Fett and Burk also suggest that the warming of the boundary layer might be caused by downward turbulent mixing of potentially warmer air from aloft, although they propose no precise way in which this mixing could occur. It may be that a hydraulic jump or wave breaking, as proposed here, is the source of such mixing. With top mixing as the heating mechanism, the thermal wake hypothesis fits the available data and agrees in one sense with our momentum wake hypothesis; that is, a hydraulic jump controlled by the mountain height is central to both theories. The two theories could be tested if more detailed wind and temperature data were available for various altitudes in the far wake.

A complete defense of the thermal wake hypothesis should explain how a positive temperature anomaly could persist for the time required for the wake air to advect 300 km downstream. The warm, less dense layer of air would have a tendency to rise and be replaced by cooler air converging from the sides of the wake, and a tendency to be eroded by enhanced convection.

In later sections, we will assume that the momentum wake hypothesis is correct, although we cannot rule out the thermal wake mechanism.

7. Numerical simulation

In this section, we undertake to deepen our understanding of St. Vincent's wake by simulating it with two numerical models. The use of two different models will provide insight into the model dependence of wake simulations. Except for section 7a.3, we limit ourselves to ideal fluid models with stratification but without boundary layer friction, heating, or separation. With such models, we will not be able to compare all the possible mechanisms for wake generation. Our models will, however, allow wave breaking, dissipation, and potential vorticity generation in a way that is strongly dependent on mountain height. They will also describe vertical vorticity dynamics including wake instability and eddy shedding, so that we can distinguish between weak and strong wakes.

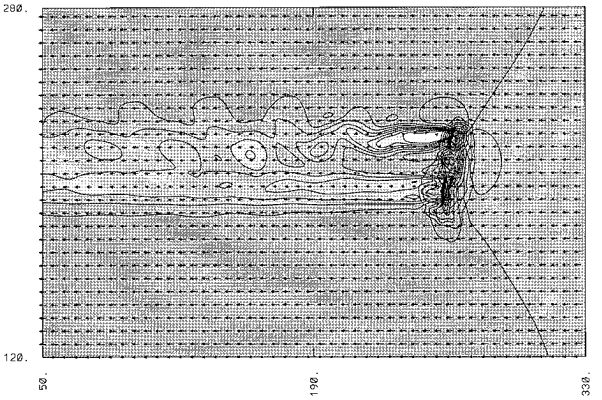

FIG. 13. Single-layer numerical calculation of the wake of St. Vincent. The wind speed is contoured with a contour interval 2 m s^{-1}. Only part of the computational domain is shown. The upstream depth, windspeed, and Froude number are 1500 m, 6.5 m s^{-1}, and 0.33, respectively. The flow is from right to left. The horizontal scale is in grid units where $\Delta x = \Delta y = 0.5$ km.

a. Single layer modeling

1) INVISCID NONROTATING SIMULATIONS

The single-layer shallow-water system described by Schär and Smith (1993a,b), Smith and Smith (1995), and Grubišić et al. (1995) has the above-mentioned characteristics. For the present application, the model was run with no bottom friction and no Coriolis force. The St. Vincent topography was digitized from a topographic map and smoothed with a 2-km influence function. Our numerical calculation is done on a 400 × 400 grid with grid element of 0.5 km. The velocity field in a 280 × 160 part of this domain is shown in Fig. 13. The free parameters in the model were chosen as follows. The depth of the layer was chosen to be $H = 1500$ m to represent the stable stratification between 600 and 2500 m (Fig. 11a). The effective gravity (g') was determined from the increase in potential temperature across this layer ($\Delta\theta = 8$°C, so that $g' = g\Delta\theta/\theta \approx 0.26$ m s^{-2}). The typical upstream windspeed $U_\infty = 6.5$ m s^{-1} was estimated from the Barbados soundings and checked with the climatology of Sadler et al. (1987). With $U_\infty = 6.5$ m s^{-1}, the ambient Froude number is

$$\mathrm{Fr} = \frac{U}{\sqrt{g'H}} = \frac{6.5}{\sqrt{(.26)(1500)}} = 0.33.$$

With a mountain height of 1000 m, the nondimensional mountain height is $M = h/H = 1000/1500 = 0.67$. According to the regime diagram in Schär and Smith (1993a), these parameters will allow hydraulic jump formation and a weak straight wake. This prediction is confirmed in Fig. 13. To test the sensitivity of the result to mountain height, the run was repeated with the moun-

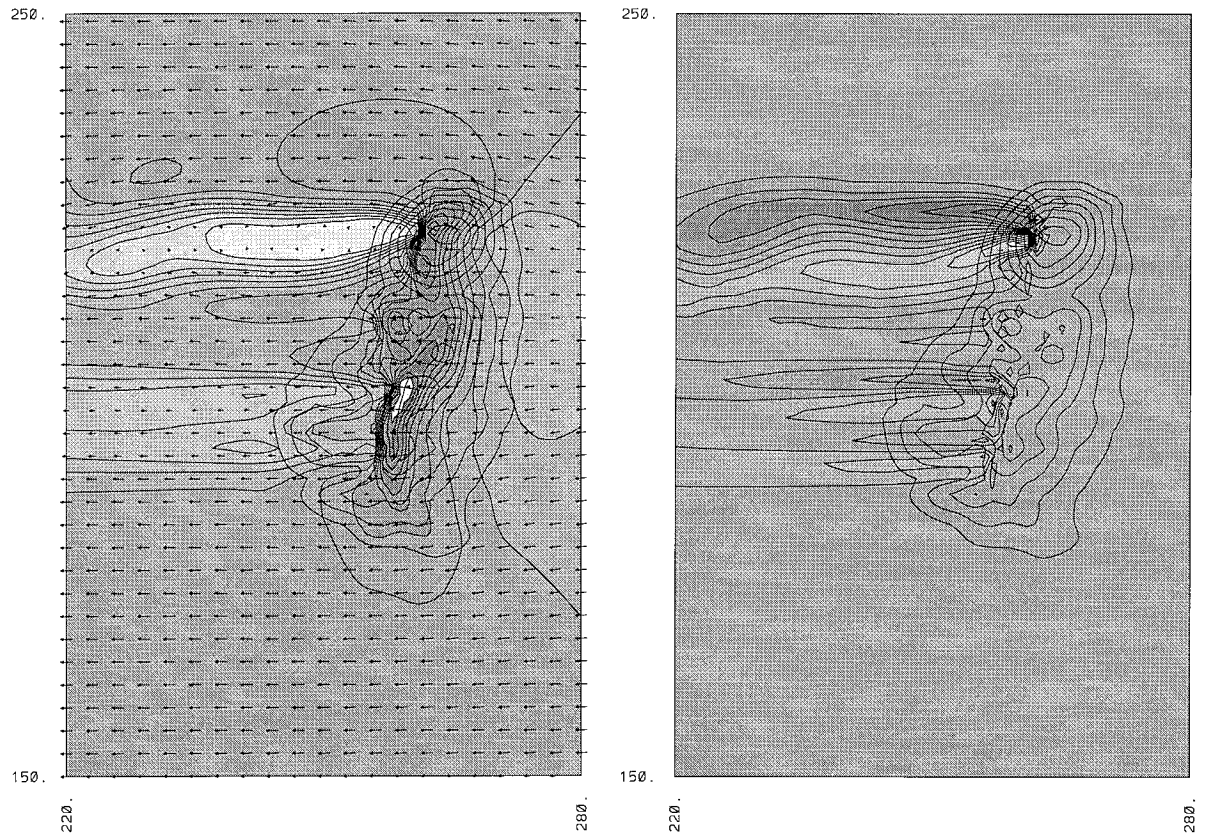

FIG. 14. Zoom view of the single-layer numerical calculation shown in Fig. 13: (a) windspeed and (b) vorticity. The horizontal scale is in grid units where $\Delta x = \Delta y = 0.5$ km.

tain height first decreased to $h = 600$ m, and then increased to $h = 1400$ m. In the former case, no wake was formed. In the latter, a strong wake was formed that exhibited eddy shedding. This result is an important confirmation of the ability of a single layer model to capture the influence of mountain height on wake type, as seen in the sunglint images.

Some of the details of the wake formation process can be seen in the zoom views shown in Fig. 14. The speed (Fig. 14a) is reduced upstream of the island and increased at the north and south capes. Such blocking and corner winds were seen in the sunglint images described in section 3. The greatest wind speed occurs over the island, just downstream of the crest line. Here the flow becomes locally supercritical (i.e., $Fr > 1$) and then encounters a hydraulic jump. The dissipation in the jump is responsible for the reduced flow speed in the wake.

The irregularity of the St. Vincent topography is evident in the near wake, particularly in the jet of wind that has passed through the notch south of Soufriere (Fig. 3). The weakest winds are in the subwake of Soufriere, as observed in the boat survey (Fig. 10). The ability of the single-layer model to capture these effects of the variable ridgeline altitude is additional evidence that it contains the essential physics.

The vorticity field (Fig. 14b) shows that the vorticity generation occurs at the location of the jumps. The two strongest speed maxima over the lee slopes (Fig. 14a) each have wake vorticity banners that form at the north and south ends of their respective jumps.

In summary, the single-layer model, with reasonably chosen parameters, qualitatively captures several features of St. Vincent's wake. This agreement suggests that the processes included in the model, for example, flow acceleration and descent over the crest followed by a dissipative hydraulic jump, may be occurring in the real atmosphere.

2) WAKE GEOSTROPHY

To confirm the conclusion in section 6a about the Coriolis effect, we have performed a few inviscid shallow-water runs to examine the approach to geostrophy. This is done by introducing the Coriolis force into the governing equation along with a constant lateral pressure gradient force to geostrophically balance the mean flow. With realistic parameters, no effect of the Coriolis force could be seen near the mountain. Downstream of the obstacle, however, the height and velocity fields in the wake were slightly altered, returning them to geostrophy. The free surface took on a cross-flow ''N'' pat-

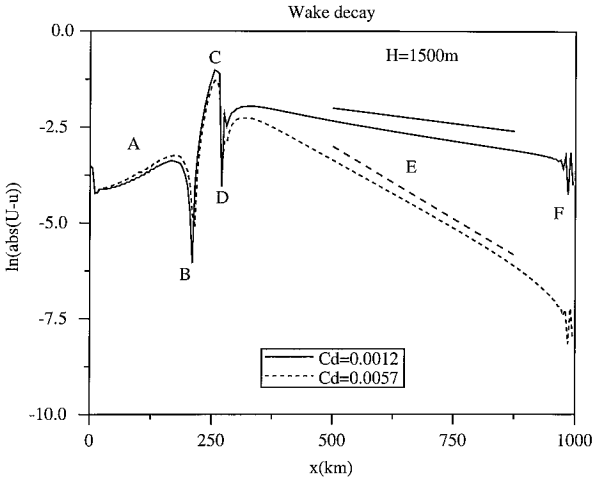

FIG. 15. The centerline velocity deficit ($u' = U - U_\infty$) from a pair of shallow-water simulations. The deficit is plotted on a log scale to reveal the exponential wake decay caused by a pressure gradient and quadratic friction. Two runs are shown with different surface drag coefficients: $C_D = 0.0012$ and 0.0057, both with a fluid depth of 1500 m. Both runs are for a circular bell-shaped mountain with $M = 0.47$ and Fr = 0.5. Labels: (a) upstream deceleration, (b) zero crossing as acceleration begins over the hill, (c) downslope acceleration, (d) zero crossing in the jump, (e) exponential wake decay, and (f) boundary errors. The straight line segment located just above each curve is the predicted slope from (2b) and (3).

tern with $\partial H/\partial y < 0$ in the wake and $\partial H/\partial y > 0$ on each side. The velocity was low in the wake and slightly higher than ambient in bands on either side. As expected, because the Rossby radius $L_R \gg a_y$, the modification to the height field dominated the geostrophic rebalancing. The difference in wake velocity between the nonrotating and rotating simulations was barely detectable.

3) BOTTOM FRICTION

To confirm the conclusion in section 6a concerning frictional control of the wake length, two shallow-water runs were carried out with bottom friction and a balancing pressure gradient. We chose a circular hill with parameters $H = 1500$ m, $M = 0.47$, and Fr = 0.5. The centerline (y = 0) velocity profiles are shown in Fig. 15. For $C_D = 0.0012$ the wake decays very slowly, while for $C_D = 0.0057$ the decay is much faster. The theoretical predictions from (2b) $L = H/(2C_D) = 624$ km and $L = 132$ agree well with the observed logarithmic slopes.

b. Continuous stratification modeling

The numerical model used in this part of the study is the semi-Lagrangian/Eulerian model described in Smolarkiewicz and Margolin (1994, 1996). The model represents a finite-difference approximation to the anelastic nonhydrostatic equations of atmospheric motion cast in the standard nonorthogonal terrain-following system of coordinates (Gal-Chen and Somerville 1975). The model is distinguished by its two-time-level temporal discretization, employing consistently the same nonoscillatory forward-in-time transport methods for all model variables and is fully second-order accurate in space and time. In this study, we have used the Eulerian variant of the model.

We modeled the airflow past St. Vincent as an adiabatic, nonrotating, dry, density-stratified fluid flow. In the runs reported here, there was no drag nor fluxes of heat and moisture at the lower boundary. The model equations include the optional subgrid-scale turbulence parameterization based on the first-order theory of Lilly (1962) and Smagorinsky (1963) for an isotropic 3D turbulence. It involves a computation of the divergence of a turbulent stress tensor and heat flux in the momentum and entropy equations, respectively. The turbulent stress and the heat transport are assumed proportional to the mean gradients by (variable) eddy viscosity and diffusion coefficients. The eddy mixing coefficients (assumed equal for heat and momentum) depend on the grid separation and the local Richardson number. The subgrid-scale mixing is locally activated for Ri < 1.

The model covers a horizontal domain of 180×160 km^2 with a uniform mesh of 90×80 grid points and a depth of 6 km covered by 60 vertical layers. The lateral absorbers occupy 10 grid points adjacent to the boundaries, whereas the top absorber occupies the upper third of the model domain. The St. Vincent topography was smoothed to a 2-km resolution. In the smoothing process, the maximum terrain height was reduced from 1000 to 700 m. The island is placed 60 km downwind from the inflow boundary. The initial potential temperature profile is the typical Barbados sounding discussed in section 4. In the control experiment, the undisturbed trade wind is represented with a uniform 4.5 m s^{-1} easterly flow. This slightly slower wind speed is used to account for the 30% reduction of the topographic height. With these parameters and an average buoyancy frequency, the nondimensional mountain height is $\hat{h} =$ hN/U $= 1.7$. To test the sensitivity with respect to $\hat{h}$, we have carried out several additional runs with $U =$ 10.5, 9, 6.5, and 3.5 m s^{-1} giving $\hat{h} = 0.7$, 0.8, 1.1, and 2.1, respectively. The basic numerical setup did not include the subgrid-scale turbulence parameterization. All runs were integrated for 6 h, which was long enough to reach the steady state, if such existed. Two experiments, with $\hat{h} = hN/U = 1.7$ and 1.1, exhibited weak unsteadiness throughout the entire integration period. To investigate the origin of this unsteadiness, the integrations were extended for an additional 6 and 8 h, respectively. To examine the sensitivity of the model solutions to the use of the turbulence parameterization, two additional experiments for $\hat{h} = hN/U = 1.7$ and 1.1 were performed including the subgrid-scale mixing. In the following, we shall discuss results from the two $\hat{h} = 1.7$ (control) experiments: with (TP) and without (nTP) the turbulence parameterization.

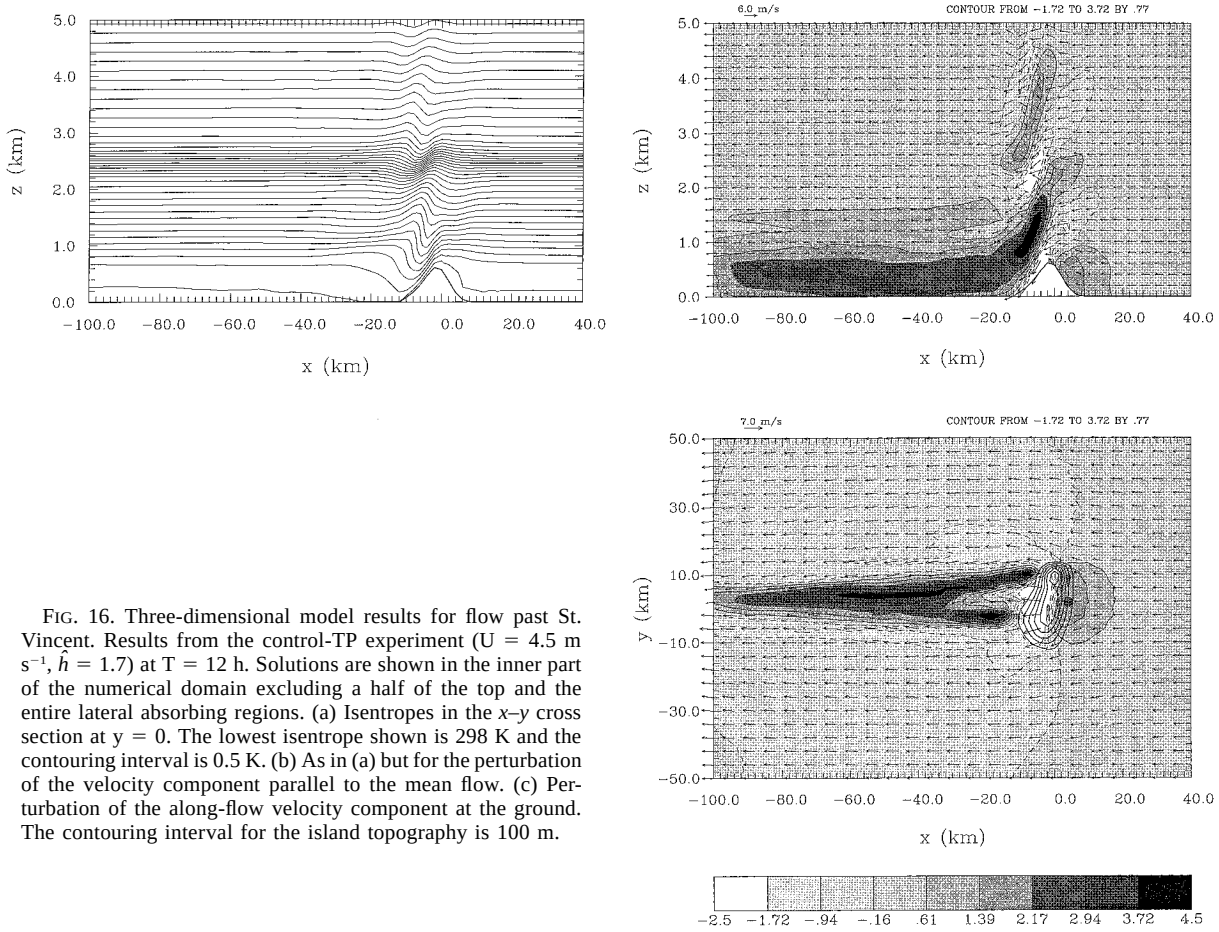

FIG. 16. Three-dimensional model results for flow past St. Vincent. Results from the control-TP experiment (U = 4.5 m s^{-1}, $\hat{h}$ = 1.7) at T = 12 h. Solutions are shown in the inner part of the numerical domain excluding a half of the top and the entire lateral absorbing regions. (a) Isentropes in the *x*–*y* cross section at y = 0. The lowest isentrope shown is 298 K and the contouring interval is 0.5 K. (b) As in (a) but for the perturbation of the velocity component parallel to the mean flow. (c) Perturbation of the along-flow velocity component at the ground. The contouring interval for the island topography is 100 m.

Figure 16 displays the steady-state solution from the control-TP experiment at T = 12 h, three hours after the wake has reached its full length. This solution captures many of the observed characteristics of the flow past St. Vincent. The long straight wake with weak winds is particularly notable (Fig. 16c). As in the 2D solution (Fig. 12), the descent of isentropes over the island involves stratification within the cumulus layer and not the inversion itself (Fig. 16a). The air in the near wake is warm, connected with the descent of isentropes and the mixing of potentially warmer air from aloft. Figure 16b shows the coexistence of a vertically propagating wave above the island with an accelerated flow over the lee slopes and a deep zone of a decelerated fluid farther downstream. At the ground, the jet south of Soufriere as well as the acceleration of the flow outside the wake are visible (Fig. 16c).

To infer the relation between the overturning wave aloft and the wake, we have examined the temporal evolution of the flow in the control-TP and -nTP experiments. In addition, we have also tested the sensitivity of the model to slight changes in mountain height. The appearance of the wake in the two control runs follows a buildup and steepening of a hydrostatic mountain wave that reaches its maximum amplitude and breaks right above the lee slope. The wake in the lee of the obstacle forms as the decelerated region from the wave breaking region starts descending toward the ground (Crook et al. 1990; Miranda and James 1992). In the nTP experiment, the descent of the decelerated region is concomitant with a collapse of the mountain wave, whereas in the TP experiment a critically steepened wave remains in place. Consequently, the solution in the nTP experiment remains weakly unsteady even after the wake reaches its full length as a buildup and collapse cycle continues, requiring several hours for the wave to regain its maximum strength. Overall, the two solutions agree in the sense that both predict weak long wakes. However, in the nTP experiment, the velocity deficit in the wake is stronger, the wake has a more irregular appearance, and, most importantly, it does not reach the ground. Instead, a shallow layer of accelerated fluid extends far downstream. We conclude that the effect of the turbulence parametrization on the model solutions is nontrivial. The mixing reduces the downstream extent of the accelerated lee-slope flow, brings

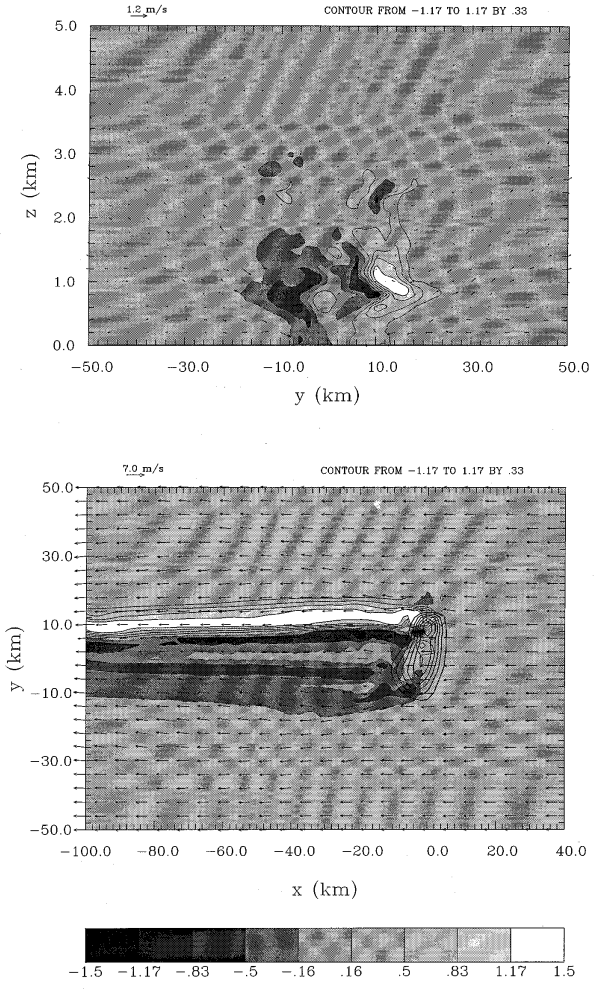

FIG. 17. Potential vorticity (PVU) in a flow past St. Vincent from the control-TP experiment at (a) in the *y*–*z* cross section 60 km downwind of the island and (b) $z = 1100$ m.

the wake down to the ground, and eliminates the collapse of the mountain wave.

To test the sensitivity with respect to $\hat{h}$, experiments were performed with $\hat{h} = 0.7$, 0.8, 1.1, and 2.1. In the first case, a deep mountain wave is present, but there is no breaking and no wake. In the last case, two short wakes with strong reverse flow exist in the lee of the island, one behind Soufriere and the other behind the mid-island ridge. The two middle runs exhibit wakes as well, providing for a continuous transition from a no wake to a strong wake regime.

Lastly, we examine the generation of PV given by $\text{PV} = (1/\rho)\vec{\boldsymbol{\xi}} \cdot \boldsymbol{\nabla}\theta$. Potential vorticity is an important wake diagnostic in stratified flow as its conservation law (i.e., $D\text{PV}/Dt = 0$) in ideal flow gives the wake fluid its permanent signature. Figure 17 shows the potential vorticity field from the -TP control run. In Fig. 17a, the PV in the wake is shown in a cross section at $x = -60$ km. In Fig. 17b, the PV at $z = 1100$ m takes the form of elongated banners of positive and negative PV that originate near the island. The PV in these banners must have its origin in the wave breaking region since the air parcels at this elevation have never come in contact with the island surface, the only other likely source of PV.

8. Discussion

In this paper, we have investigated weak mountain wakes of the Windward Islands, with the wake of St. Vincent as a prototype. Weak wakes are caused by mountains just high enough to cause gravity wave breaking. Most of our information comes from qualitative interpretations of GOES and Landsat sunglint images. These images show a straight and extraordinarily long region of smooth sea surface downwind of St. Vincent, which we interpret as a deep atmospheric wake with reduced wind speed. The length of the wake exceeds 300 km and appears to be unaffected by diurnal heating of the island.

In addition to the satellite images, boat surveys and low-level aircraft surveys were used to investigate the field of airflow close to the island. The boat surveys near St. Vincent confirmed the wake behind Soufriere, the sharp wind shear at the edge of the wake, and the embedded jet seen in the sunglint images. The aircraft surveys showed that the wake air is warm and dry, and revealed the descent of warm dry air over the island.

A key property of weak wakes is their sensitivity to variations in the mountain ridgeline. This sensitivity is due to the fact that weak wakes form under conditions where the terrain is only just high enough to create a wake. The island of Barbados and the southern part of Martinique fall below this threshold. The islands of Dominica, northern Martinique, southern St. Lucia, and St. Vincent exceed the threshold. A related result of this sensitivity is the occurrence of fine structure in the near wakes—jets and wakes caused by ridgeline irregularities. All the Windward Islands have examples of this fine structure in their sunglint images.

The great length of St. Vincent's wake is evidence of inefficient entrainment of momentum at the top and sides of the wake. The remaining wake decay mechanism, acceleration by the regional pressure gradient, would give a wake length of $L = H/(2\,C_D)$. The agreement of this value with the observed wake length provides support for the pressure gradient mechanism.

Somewhat surprisingly, the single-layer shallow-water model captures some essential aspects of weak wake dynamics. This model generates a wake by first accelerating the flow and then decelerating it rapidly in a hydraulic jump that forms over the lee slope. The dissipation in these jumps generates weak banners of vorticity that advect downstream to form the edges of the wakes. The single-layer model also predicts the upstream blocking, the corner winds, the near wake valley jet, and the long straight wake found in the St. Vincent observations. With bottom friction added, the

shallow-

water model illustrates the pressure gradient wake decay mechanism.

Another view of wake generation is afforded by our fully three-dimensional ideal-fluid numerical simulation with a subgrid turbulence parameterization. When the control parameters are chosen appropriately, wave breaking above the lee slope generates PV banners that trail downstream, advected by the mean flow. The 3D model also captures the descent of the cumulus-layer air, the upstream blocking, the corner winds, and the jet through the valley south of Soufriere. The predicted wake depth is about 800 m.

The primary conclusion of our study is that weak wakes are common, robust, and long lived in atmospheric flow, but they are sensitive to mountain height. According to our models, weak wakes are created by stratification-induced dissipation, so-called wave breaking, and are closely connected with PV generation. Several questions regarding weak wakes are left unanswered however. We were not able to determine the shape and location of the dissipative region over the island that generates St. Vincent's wake, nor the nature of the heat, momentum, and moisture fluxes within that region. We do not know the relative importance of wave breaking and surface roughness in creating the dissipative zones. We have not documented, by direct observation, the acceleration of the air over the ridge crest, although this phenomenon has been observed elsewhere (Smith 1987). We do not know the depth of the wake, nor how it evolves downstream.

Acknowledgments. Dennis Chesters at NASA/GSFC helped us to obtain the GOES imagery. Christoph Schär allowed us to use his shallow-water model. Sigrid R.-P. Smith assisted with the field project logistics. Paul Gravel and other personnel at SVG Air assisted with the aerial surveys. Mr. Lion King and his crew assisted with the boat surveys. Steve Burk helped clarify the heating hypothesis for wake longevity. Teddie Keller and Peter Neilley offered useful comments on the manuscript. Qingfang Jiang assisted with numerical experiments with friction and Coriolis force. The image analysis was carried out at the Yale Center for Earth Observation. This research was supported by National Science Foundation Grant ATM-8914138 and by the Office of Naval Research Grant N00014-93-1-0238, under the Marine Meteorology Program. Vanda Grubišić acknowledges support of the Advanced Study Program at NCAR while doing this research. NCAR is sponsored by the National Science Foundation.

REFERENCES

Barr, S., 1982: Skirt clouds associated with the Soufriere eruption of 17 April 1979. *Science,* **216,** 1111–1112.

Blumen, W., 1972: Geostrophic adjustment. *Rev. Geophys. Space Phys.,* **10,** 485–528.

Chopra, K. P., 1973: Atmospheric and oceanic flow problems introduced by islands. *Advances in Geophysics,* Vol. 16, Academic Press, 298–416.

Clark, T. L., and W. R. Peltier, 1977: On the evolution and stability of finite amplitude mountain waves. *J. Atmos. Sci.,* **34,** 1715–1730.

Cox, C., and W. Munk, 1954a: Statistics of the sea surface derived from sun glitter. *J. Mar. Res.,* **13,** 198–227.

——, and ——, 1954b: Measurement of the roughness of the sea surface from photographs of the sun's glitter. *J. Opt. Soc. Amer.,* **44,** 838–850.

Cram, R., and K. Hanson, 1974: The detection by *ERTS-1* of wind-induced ocean surface features in the lee of the Antilles Islands. *J. Phys. Oceanogr.,* **4,** 594–600.

Crook, A. N., T. L. Clark, and M. W. Moncrieff, 1990: The Denver cyclone. Part I: Generation in low Froude number flow. *J. Atmos. Sci.,* **47,** 2725–2741.

Deardorff, J. W., 1976: Island wind shadows observed by satellite and radar. *Bull. Amer. Meteor. Soc.,* **57,** 1241–1242.

DeSouza, R. L., 1972: A study of atmospheric flow over a tropical island. M.S. thesis, Dept. of Meteorology, The Florida State University, 203 pp.

Etling, D., 1989: On atmospheric vortex streets in the wake of large islands. *Meteor. Atmos. Phys.,* **41,** 157–164.

Fett, R. W., and K. M. Rabe, 1976: Island barrier effects on sea state as revealed by a numerical wave model and DMSP satellite data. *J. Phys. Oceanogr.,* **6,** 324–334.

——, and R. G. Isaacs, 1979: Concerning causes of anomalous gray shades in DMSP visible imagery. *J. Appl. Meteor.,* **18,** 1340–1351.

——, and W. A. Bohan, 1981: Navy Tactical Applications Guide, Vol. 3, North Atlantic and Mediterranean. NEPRF Tech. Rep. 80-07, 250 pp.

——, and S. D. Burk, 1981: Island barrier effects as observed by satellite and instrumented aircraft, and simulated by a numerical model. *Mon. Wea. Rev.,* **109,** 1527–1541.

Flammarion, C., 1874: *The Atmosphere.* Translated by J. Glaisher. Harper and Bros., 453 pp.

Fuller, W. H., Jr., S. Sokol, and W. H. Hunt, 1982: Airborne lidar measurements of the Soufriere eruption of 17 April 1979. *Science,* **216,** 1113–1115.

Gal-Chen, T., and R. C. J. Somerville, 1975: On the use of a coordinate transformation for the solutions of the Navier–Stokes equations. *J. Comput. Phys.,* **17,** 209–228.

Garstang, M., P. D. Tyson, and G. D. Emmitt, 1975: The structure of heat islands. *Rev. Geophys. Space Phys.,* **13,** 139–152.

Grubišić, V., R. B. Smith, and C. Schär, 1995: The effect of bottom friction on shallow-water flow past an isolated obstacle. *J. Atmos. Sci.,* **52,** 1985–2005.

Hubert, L. F., and A. F. Krueger, 1962: Satellite pictures of mesoscale eddies. *Mon. Wea. Rev.,* **90,** 457–463.

Huppert, H. E., and J. W. Miles, 1969: Lee waves in stratified flow. Part 3: Semi-elliptical obstacles. *J. Fluid Mech.,* **35,** 481–496.

Johnson, D. B., P. Flament, and R. L. Bernstein, 1994: High-resolution satellite imagery for mesoscale meteorological studies. *Bull. Amer. Meteor. Soc.,* **75,** 5–33.

Khattak, S., R. A. Vaughan, and A. P. Cracknell, 1991: Sunglint and its observation in AVHRR data. *Remote Sens. Environ.,* **37,** 101–116.

Lilly, D. K., 1962: On the numerical simulation of buoyant convection. *Tellus,* **14,** 148–172.

McClain, E. P., and A. E. Strong, 1969: On anomalous dark patches in satellite-viewed sunglint areas. *Mon. Wea. Rev.,* **97,** 875–884.

Maul, G. A., and H. R. Gordon, 1975: On the use of the Earth Resources Technology Satellite (LANDSAT-1) in optical oceanography. *Remote Sens. Environ.,* **4,** 95–128.

Miranda, P. M., and I. N. James, 1992: Non-linear three-dimensional effects on gravity wave drag: Splitting flow and breaking waves. *Quart. J. Roy. Meteor. Soc.,* **118,** 1057–1081.

Needham, B. H., 1976: Observation of wind-induced sea surface

feature off Pulu Bawean, Java, from LANDSAT-1. *Bull. Amer. Meteor. Soc.,* **57,** 444–448.
Sadler, J. C., M. A. Lander, A. M. Hori, and L. K. Oda, 1987: *Tropical Marine Climatic Atlas.* Vol. I, *Indian Ocean and Atlantic Ocean.* Department of Meteorology, University of Hawaii, 52 pp.
Schär, C., 1993: A generalization of Bernoulli's theorem. *J. Atmos. Sci.,* **50,** 1437–1443.
——, and R. B. Smith, 1993a: Shallow-water flow past isolated topography. Part I: Vorticity production and wake formation. *J. Atmos. Sci.,* **50,** 1373–1400.
——, and ——, 1993b: Shallow-water flow past isolated topography. Part II: Transition to vortex shedding. *J. Atmos. Sci.,* **50,** 1401–1412.
Siebesma, A. P., and J. W. M. Cuijpers, 1995: Evaluation of parametric assumptions for shallow cumulus convection. *J. Atmos. Sci.,* **52,** 650–666.
Smagorinsky, J., 1963: General circulation experiments with the primitive equations. I. The basic experiment. *Mon. Wea. Rev.,* **91,** 99–164.
Smith, R. B., 1985: On severe downslope winds. *J. Atmos. Sci.,* **42,** 2597–2603.
——, 1987: Aerial observations of the Yugoslavian Bora. *J. Atmos. Sci.,* **44,** 269–297.
——, 1989a: Hydrostatic flow over mountains. *Advances in Geophysics,* Vol. 31, Academic Press, 1–41.
——, 1989b: Comment on ''Low Froude number flow past three dimensional obstacles. Part I: Baroclinically generated lee vorticies''. *J. Atmos. Sci.,* **46,** 3611–3613.
——, 1989c: Mountain-induced stagnation points in hydrostatic flow. *Tellus,* **41A,** 270–274.
——, and S. Grønås, 1993: Stagnation points and bifurcation in 3-D mountain airflow. *Tellus,* **45A,** 28–43.
——, and V. Grubišić, 1993: Aerial observations of Hawaii's wake. *J. Atmos. Sci.,* **50,** 3728–3750.
——, and D. F. Smith, 1995: Pseudoinviscid wake formation by mountains in shallow-water flow with a drifting vortex. *J. Atmos. Sci.,* **52,** 436–454.
Smolarkiewicz, P. K., and L. G. Margolin, 1994: Variational solver for elliptic problems in atmospheric flows. *Appl. Math. Comp. Sci.,* **4,** 527–551.
——, and ——, 1996: On forward-in-time differencing for fluids: An Eulerian/semi-Lagrangian nonhydrostatic model for stratified flows. *Atmos.-Ocean.,* **34,** In press.
Stein, J., 1992: Investigation of the regime diagram of hydrostatic flow over a mountain with a primitive equation model. Part I: Two-dimensional flows. *Mon. Wea. Rev.,* **120,** 2962–2976.
Strong, A. E., and I. S. Ruff, 1970: Utilizing satellite-observed solar reflections from the sea surface as an indicator of surface wind speeds. *Remote Sens. Environ.,* **1,** 181–185.
——, R. J. DeRycke, and H. G. Stumf, 1974: Extensive areas of reduced waves leeward of the Lesser Antilles. *Geophys. Res. Lett.,* **1,** 47–49.
Turner, J. S., 1973: *Buoyancy Effects in Fluids.* Cambridge University Press, 367 pp.